Article

Influence of Gas-Flow Conditions on the Evolution of Thermally Insulating Si₃N₄ Nano-Felts

Balanand Santhosh *[ID], Mattia Biesuz [ID], Andrea Zambotti [ID] and Gian Domenico Sorarù [ID]

Glass and Ceramics Lab, Department of Industrial Engineering, University of Trento, Via Sommarive 9, 38123 Trento, Italy; mattia.biesuz@unitn.it (M.B.); andrea.zambotti-1@unitn.it (A.Z.); giandomenico.soraru@unitn.it (G.D.S.)
* Correspondence: balanand.santhosh@unitn.it

Abstract: This paper discusses the role of nitrogen (N_2) gas flow conditions on the formation of silicon nitride (Si_3N_4) nano-felts from polysiloxane-impregnated polyurethane (PU) foams. The polymeric foam was converted into an amorphous silicon oxycarbide (SiOC) artefact during pyrolysis, which was then transformed, at a higher temperature, into a Si_3N_4 felt through a reaction between the decomposition products of SiOC with N_2. The study identified that a N_2 flux of ~2.60 cm.min^{-1} at the cross-section of the furnace (controlled to 100 cm^3.min^{-1} at the inlet of the furnace using a flowmeter) substantially favored the transformation of the parent SiOC foam to Si_3N_4 felts. This process intensification step significantly reduced the wastage and the energy requirement while considering the material production on a bulk scale. The study also inferred that the cell sizes of the initial PU templates influenced the foam to felt transformation.

Keywords: silicon nitride; polymer-derived ceramics; ceramic nano-belts; nitrogen flow rate; thermal insulation

1. Introduction

The development of thermally and chemically stable materials for thermal insulation, especially for application at elevated temperatures, is of pivotal significance in the present economic and technical scenario. Usually, ceramics-based materials are deployed for these purposes owing to their low thermal conductivity and unrivalled stability [1]. Advanced research [2–5] is being conducted to develop ceramics-based ultra-light materials with 'super-insulation' properties and with very low thermal distortion. Different ceramic aerogels [6], foams [7,8], and fibrous materials [2,4] are also being studied as potential high-temperature insulants, while some are already in mass-production (www.aeropan.it, accessed on 25 January 2022), for domestic as well as industrial insulation [9].

Among the different ceramic materials in use, Si_3N_4 has lately gained interest in the community owing to its high thermal and mechanical stability, thermal shock resistance, and low dielectric constant and loss values [10–14]. Si_3N_4-based fibrous materials combining thermal insulation and refractory characteristics were recently proposed, also devising efficient approaches to shape the materials as required [14,15]. Among the different strategies, Si_3N_4 nano-felts can be obtained by the polymer-derived ceramics (PDC) route [15–17] using polyurethane (PU) as templates [15]. This approach reported a simple, robust, and flexible synthesis route to develop ultra-light, well-shaped fibrous Si_3N_4 ceramics having ultra-low thermal conductivity [15]. The controlled pyrolysis of polymeric precursor-impregnated PU-foam templates causes, at first, the formation of an amorphous SiOC foam [7,18,19], which is subsequently converted into a nano-fibrous Si_3N_4 artefact by reaction with N_2 atmosphere. The evolution process of nano-felts was reported to start with the release of SiO gas (reaction (1)) followed by the reaction of this SiO gas with

the C from the ceramic foam and the N_2 gas, leading to alpha-silicon nitride (α-Si_3N_4) (reaction (2)) [15].

$$SiO_{2\,(s)} + C_{(s)} \rightarrow SiO_{(g)} + CO_{(g)} \tag{1}$$

$$3SiO_{(g)} + 3C_{(s)} + 2N_{2\,(g)} \rightarrow Si_3N_{4\,(s)} + 3CO_{(g)} \tag{2}$$
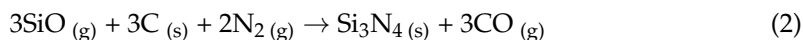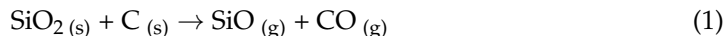
The felts were also found to have excellent chemical and thermal resistance, low thermal conductivity and mechanical performances [15], and were proposed for different applications [20,21].

The sequence of reactions (1) and (2), in order to allow the processing of an α-Si_3N_4 felt with optimum features and leading to a complete transformation of the parent SiOC foam, must be carefully controlled. Parameters such as the temperature and time, the cell size and density of the SiOC foam, and the flow rate of the reactive N_2 gas may play a key role in this process. Indeed, in a previous study conducted in our lab, some parameters (temperature, time, the precursor-to-template ratio that controls the final density of the SiOC foam, and cell size) were optimized, but the gas flow conditions on the evolution were not identified and documented. In the present study, we focused our attention on the role of the flow rate on the synthesis of the Si_3N_4 felts. In the dynamic system in which the felt is formed, the N_2 gas has two functions: (i) N_2 is a reactant and needs to be available at the reaction site that is at the surface of the struts of the foam when the struts are decomposing, liberating SiO and CO gases; and (ii) N_2 needs to act as a carrier gas to remove CO from the reaction site, allowing the decomposition to proceed further. Obviously, if the N_2 gas is fed to the system at too slow a rate, reaction (2) may not proceed, because of the scarcity of reactants or because the CO is not removed fast enough and reaction (1) does not proceed. On the other hand, if the N_2 flow is too high, it could remove not only CO but also SiO, before SiO could react to form the desired α-Si_3N_4. Hence, extended understanding and optimization of the reported fabrication process [15], considering the flow parameters, is essential to fine-tune the processing to befit the different applications envisioned.

In this work, the influence of the gas flow parameters on the evolution of Si_3N_4 nanobelts is reported. These studies were conducted using three starting PU templates of different cell features and at two different gas flow rates to rationalize the results obtained.

2. Materials and Methods

2.1. Materials

The commercially available polysiloxane SPR-036 (Starfire Systems Inc., Glenville, NY, USA, viscosity: 50–500 cps under room-temperature conditions) was used as the ceramic precursor without any further modifications. Platinum–divinyl tetramethyl disiloxane complex in xylene (CAS#: 68478-92-2; Sigma–Aldrich, Saint Louis, MO, USA) with a platinum content of ~2% (hydrosilylation catalyst) was used as the catalyst after diluting it to 0.1% Pt using p-xylene (CAS#: 106-42-3, Sigma–Aldrich, Saint Louis, MO, USA) to ensure its uniform dispersion in the system. Polyester-based PU foams (ARE- S.r.l, Rosate, Milan, Italy) were used as templates for fabricating the ceramic felts. Three types of PU foams having completely open cells but with different cell sizes were used for the study: PPI 45, PPI 60, and PPI 90 (PPI = pores per inch). The dimensions of the starting PU foams are given in Table S1 of 'Supplementary Materials'. The studies were conducted with two different PU thicknesses (t): 10 mm and 20 mm, and hereafter, they are referred to as 10 and 20 for convenience, respectively.

2.2. Processing the 'Nano-Felts'

The processing of the felts is reported in detail in the previous works [15,21]. The samples were prepared at the previously optimized condition of 1565 °C with a holding time of 4 h, with the entire processing happening in a controlled nitrogen flow. For comparison purposes, selected samples were also pyrolyzed in Ar flow using the same temperature profile. A brief process sketch is presented in Figure 1 for a basic understanding of the process. The PU: SPR 036 weight ratio was 1:2 for all the samples. All the other main

conditions were the same as what we adopted in our previous works [15,21], except for a slight modification in the flow rate of the N_2 gas. The study was conducted at two different flow rates measured using the flowmeter:

(1) low (100 $cm^3.min^{-1}$), and
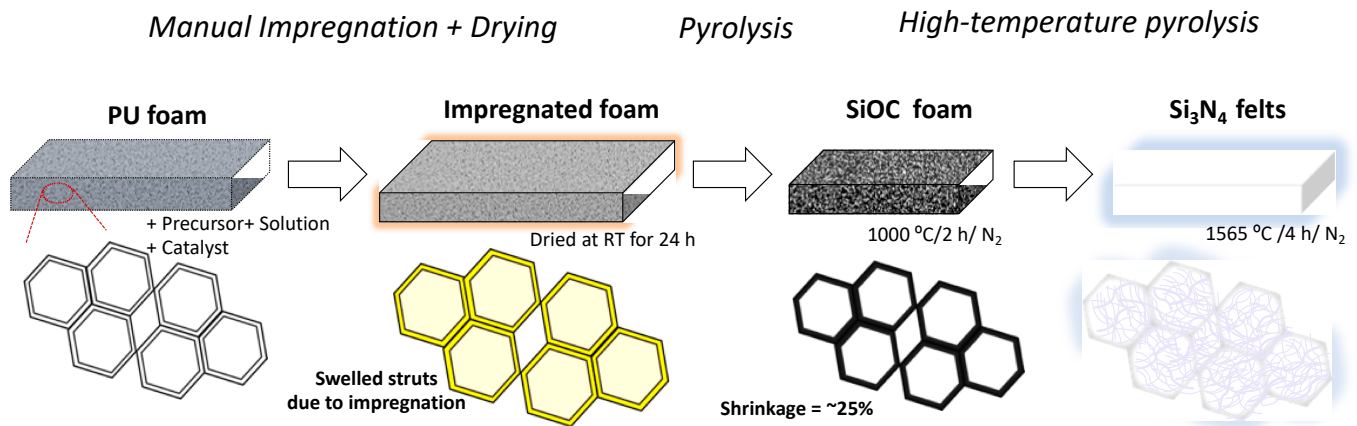(2) high (600 $cm^3.min^{-1}$).

Figure 1. Processing of the 'nano-felts'. The pyrolysis process that converts the impregnated polyurethane (PU) foam into the ceramic silicon oxycarbide (SiOC) foam is complete at ~1000 °C. Above that temperature, the ceramic foam is stable up to ~1500 °C and then it converts into the silicon nitride (Si_3N_4) felts at 1565 °C.

However, these flowrates set at the inlet of the furnace (using the flowmeter) correspond to fluxes of 2.60 $cm.min^{-1}$ (100 $cm^3.min^{-1}$) and 15.58 $cm.min^{-1}$ (600 $cm^3.min^{-1}$) at the cross-section of the furnace, considering the inner diameter of the alumina tube = 70 mm.

Nevertheless, henceforth, the two different flow rates are mostly referred to as 100 and 600 for convenience, respectively.

2.3. Material Characterizations

The bulk densities of the samples were calculated from their dimensions (measured using a Vernier caliper, sensitivity ±0.01 mm) and their weight (measured using a digital balance, sensitivity ±0.1 mg). The X-ray diffraction (XRD) spectra were collected with a D/Max- B diffractometer (Rigaku Co., Tokyo, Japan) operating at 40 kV and 30 mA with Cu Kα radiation. A digital microscope (Olympus-DSX 1000, Olympus Corp., Shinjuku City, Tokyo, Japan) was used to study the fracture surface. The scanning electron microscopy (SEM) micrographs were taken using a Supra 40 FE-SEM (Carl Zeiss NTS GmbH, Oberkochen, Germany) on the fracture surfaces after coating the samples with a thin Pt-Pd film by sputtering. The thermal diffusivities of the different felt samples were measured using the Laser Flash Analyzer, LFA 467-HyperFlash (NETZSCH-Gerätebau GmbH, Selb, Germany) in an N_2 environment. Disk-shaped samples were made to fit in the measurement slits having a diameter = 12.7 mm, the thickness of the samples was recorded, and the parallel surfaces were coated with a thin graphite film to avoid reflection of the laser energy from the surfaces.

3. Results and Discussion

Pyrolytic transformation of the siloxane-impregnated PU completes at around 1000 °C [19], when a SiOC foam is formed. Silicon oxycarbides are complex amorphous materials formally consisting of a $SiO_2/SiC/C$ mixture. The SiOC is stable in inert atmosphere up to ca. 1400 °C. At higher temperatures, a decomposition usually occurs due to the carbothermal reduction of the silica component with the formation of SiO and CO gases [22]. In the present experiments, the temperature was increased up to 1565 °C, with

a dwell for 4 h, and the XRD patterns recorded on the samples treated in N_2 and Ar are reported in Figure 2. While pyrolysis in N_2 results in the formation of Si_3N_4 (α-Si_3N_4 forms the primary crystalline phase; however, traces of a β-Si_3N_4 secondary phase can also be seen as small peaks on the diffractogram [15]), the one in Ar instead caused the formation of β-SiC (a small shoulder to the β-SiC peak at 35°, which can be seen at around $2\theta = 33$–35°, can be assigned to the stacking faults in β-SiC [18]) (see Figure 2).
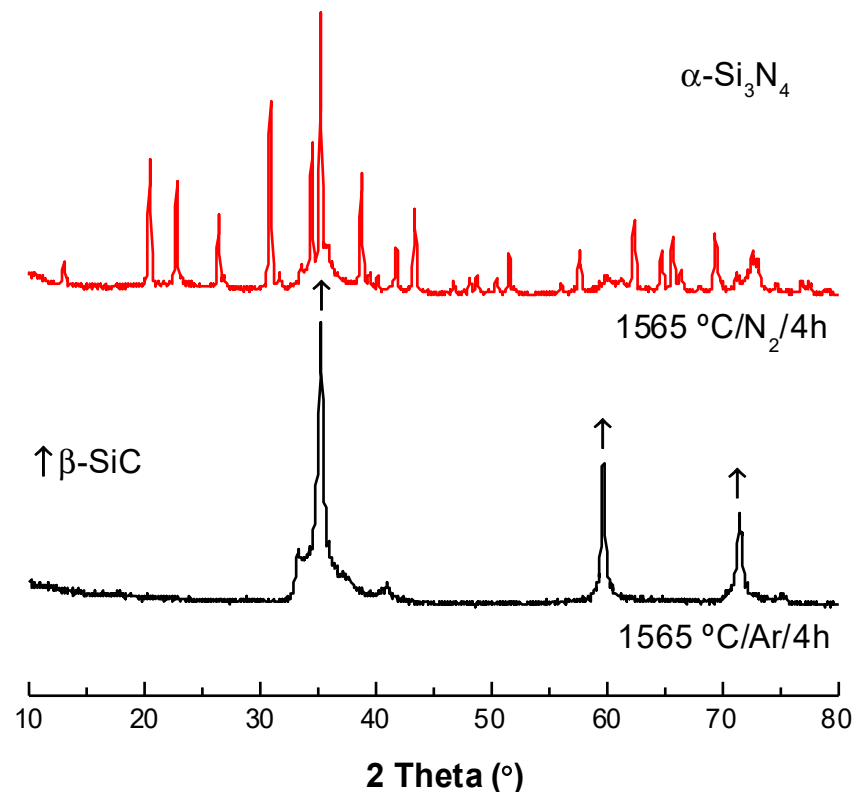

Figure 2. X-ray diffraction (XRD) patterns of the samples prepared in argon (Ar) and nitrogen (N_2) atmospheres, under the same heat treatment conditions.

This result can be explained considering the two-step formation process of silicon nitride as described previously: first, SiO_2 reacts with C to form $SiO_{(g)}$ and $CO_{(g)}$ reaction (1); then, the reaction between $SiO_{(g)}$, $C_{(s)}$, and $N_{2(g)}$ leads to the formation of silicon nitride and additional CO reaction (2). However, when the process is carried out in Ar, the second reaction cannot take place, due to the lack of N_2 in the atmosphere. Hence, according to [23], SiO can react with carbon to form SiC + CO reaction (3):

$$SiO_{(g)} + 2C_{(s)} \rightarrow SiC_{(s)} + CO_{(g)} \tag{3}$$
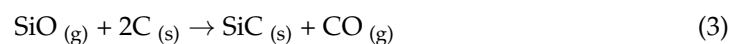
The density, volume shrinkage, and mass loss of the felt samples prepared at the different flow rates of N_2 are given in Table 1. The density was found to vary in the range of 0.04–0.06 g.cm^{-3}. The flow condition and the thickness of the PU templates showed only a marginal influence on the densification and the mass loss occurring. The volume shrinkage was found to increase (in general) with the thickness of the PU foams used. However, these macroscopic data were irreconcilable with the visual observation of the felts developed. It was observed that samples prepared at the highest flow rates of N_2 (600) were found to have some darker regions, which confirm the nonuniform transformation of the foams to felts under the previously optimized conditions (see Figure 3).

Table 1. The bulk density, volumetric shrinkage, and mass loss (%) of nano-felts samples prepared with different PPIs, having varied thicknesses, and under different N_2 flow conditions.

PU Foam	PU Foam Thickness (mm)	N_2-Flow Conditions (cm^3.min^{-1})	Bulk Density (g.cm^{-3})	Volume Shrinkage (%)	Mass Loss (%)
PPI 90	10	100	0.05	55.3	67.2
	20	100	0.06	52.5	64.4
	10	600	0.04	51.6	68.0
	20	600	0.04	53.5	69.3
PPI 60	10	100	0.04	42.0	72.4
	20	100	0.04	48.1	70.7
	10	600	0.04	49.1	67.6
	20	600	0.05	49.6	65.4
PPI 45	10	100	0.04	47.6	69.2
	20	100	0.04	51.4	70.8
	10	600	0.04	41.7	70.9
	20	600	0.05	47.9	66.0

The evolution of these nano-felts was further studied by investigating the fractured surfaces using SEM (see Figure 4). On studying the samples prepared at a higher flow rate (600 cm^3.min^{-1}), remnants of the foams were observed in the felts matrix, which were previously observed to be the dark patches on the pictures of the felts (Figure 3). This observation was clearer in the case of the samples prepared from the PUs having the larger cell-window sizes, viz. PPI 45 and PPI 60 (from the SEM images, see Figure 4). Meanwhile, the felts samples prepared from PU-PPI 90, having smaller cell-window sizes were better-transformed with less foam residues even at a flow rate of 600 cm^3.min^{-1}. Closer observations of the felts from different PPIs (on samples prepared at 600 cm^3.min^{-1}) using digital microscopes further support this observation (see Figure 5), i.e., more untransformed relics can be seen for the samples from PPI 45 and PPI 60 than those from PPI 90. However, the samples prepared at the lower flow rates were well transformed with literally no observable relics of the foams. These observations confirm that the PPIs and flow rates together play a role in determining the transformation degree of the foams into Si_3N_4 felts. We can rationalize the experimental results as follows. The high flow rates of N_2 increase the rate of removal of $SiO_{(g)}$, formed through reaction (1), from the reaction site where it should combine, through reaction (2), with N_2 and C to form Si_3N_4, reducing, accordingly, the transformation yield. Similarly, the smaller cell size (as in PPI 90) helps retain the SiO better than the larger cell sizes, as PPI 45 and PPI 60 (see Figure 5). In summary, preventing SiO from diffusing out of the foam, either by decreasing the N_2 flow rate or decreasing the cell size of the starting PU foam, before it can react to form Si_3N_4, helps in obtaining a better transformed felt.
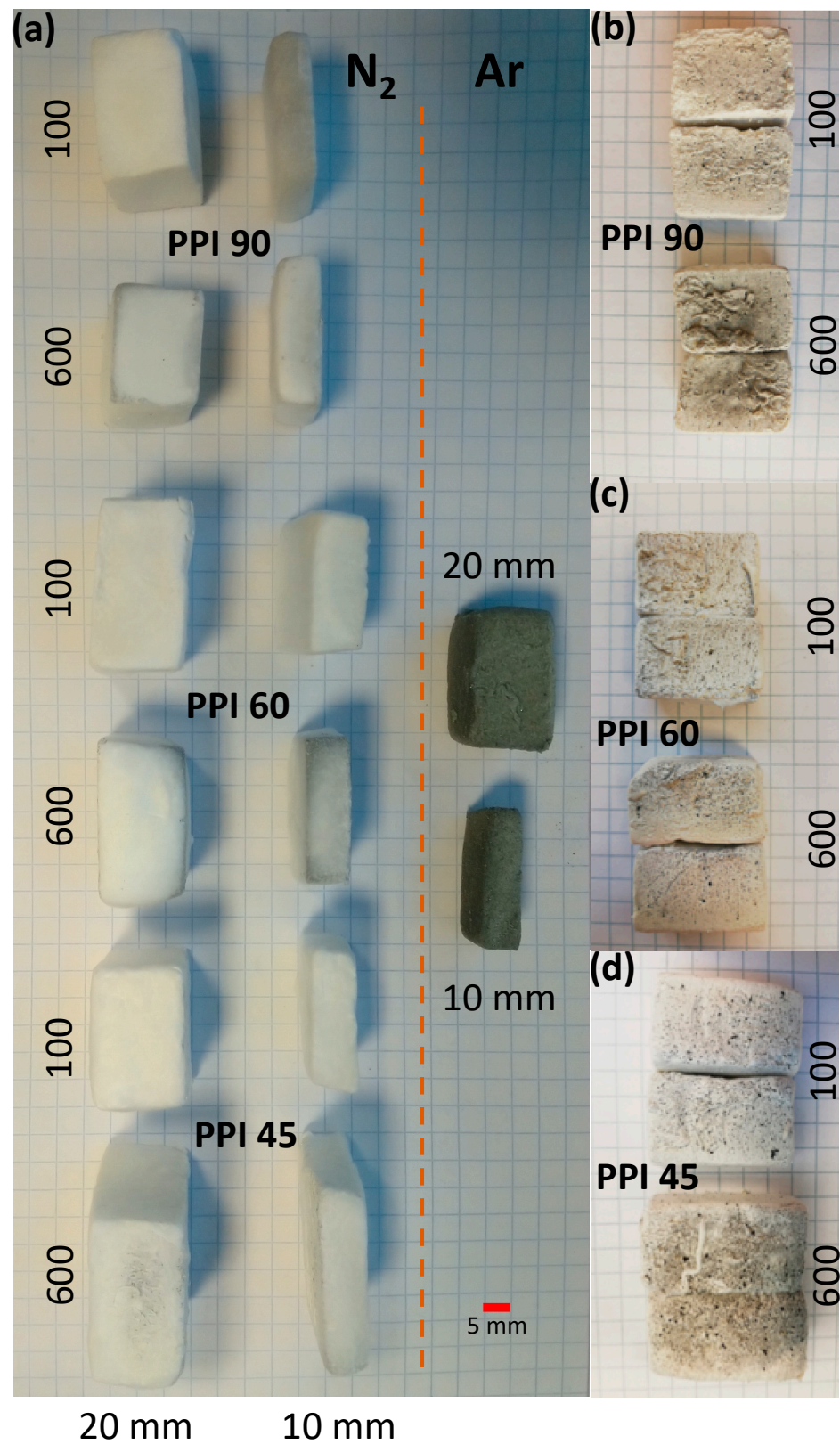
Figure 3. Pictures of felt samples (**a**) prepared from different PU PPIs and thicknesses, at different flow rates of N_2 along with the control sample prepared in Ar (PPI 90, 1:2, 100 cm^3.min^{-1}), and sectioned view of the felts prepared (demonstrated using samples prepared using 20 mm PUs) at 100 cm^3.min^{-1} and 600 cm^3.min^{-1}, (**b**) PPI 90, (**c**) PPI 60, and (**d**) PPI 45.
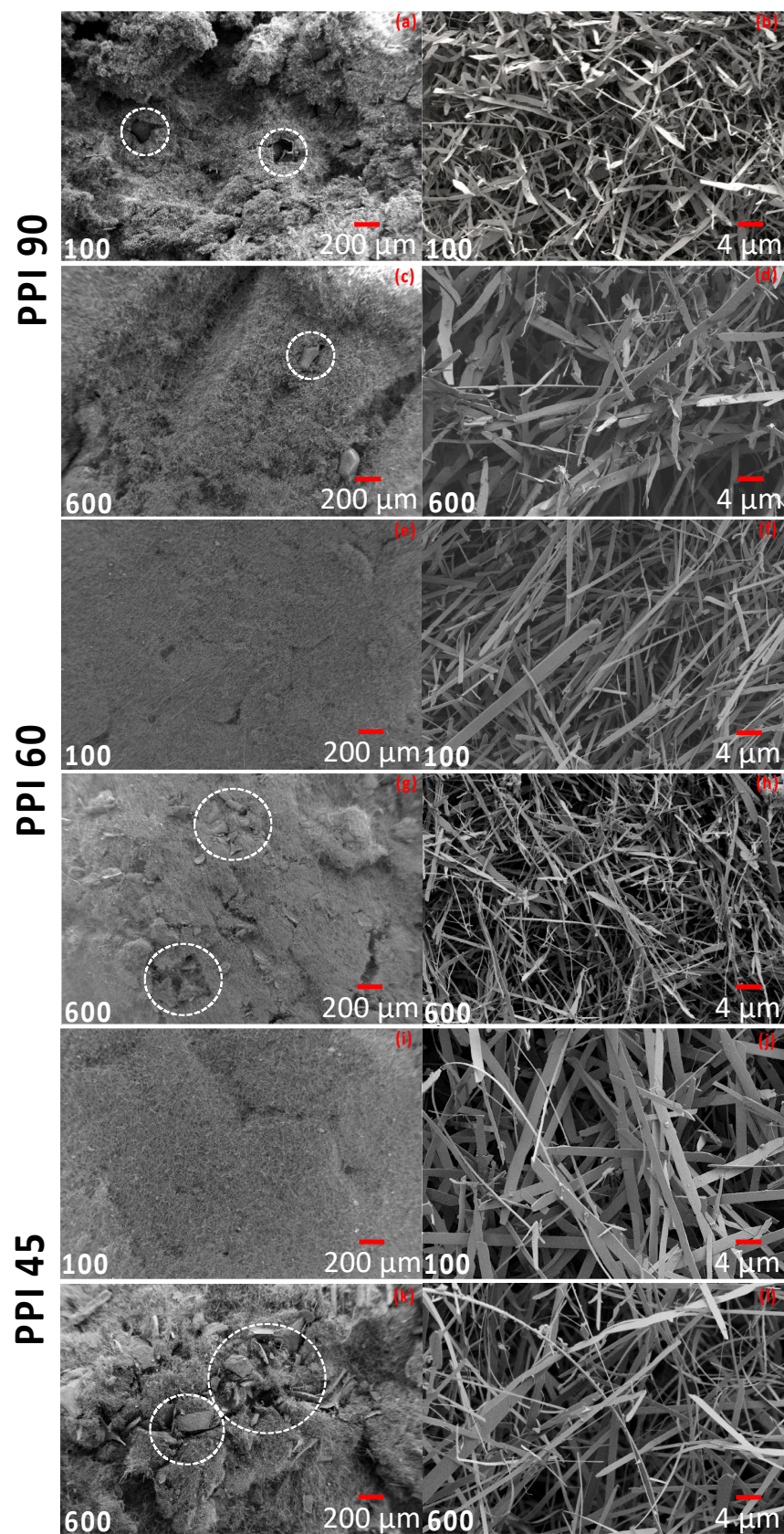
Figure 4. SEM micro-images of felts prepared from (**a–d**) PPI 90, (**e–h**) PPI 60, and (**i–l**) PPI 45 at N_2 flow rates of 100 $cm^3.min^{-1}$ and 600 $cm^3.min^{-1}$ (images from samples prepared using 20 mm PUs; the relicts of the SiOC foams are shown in circles).

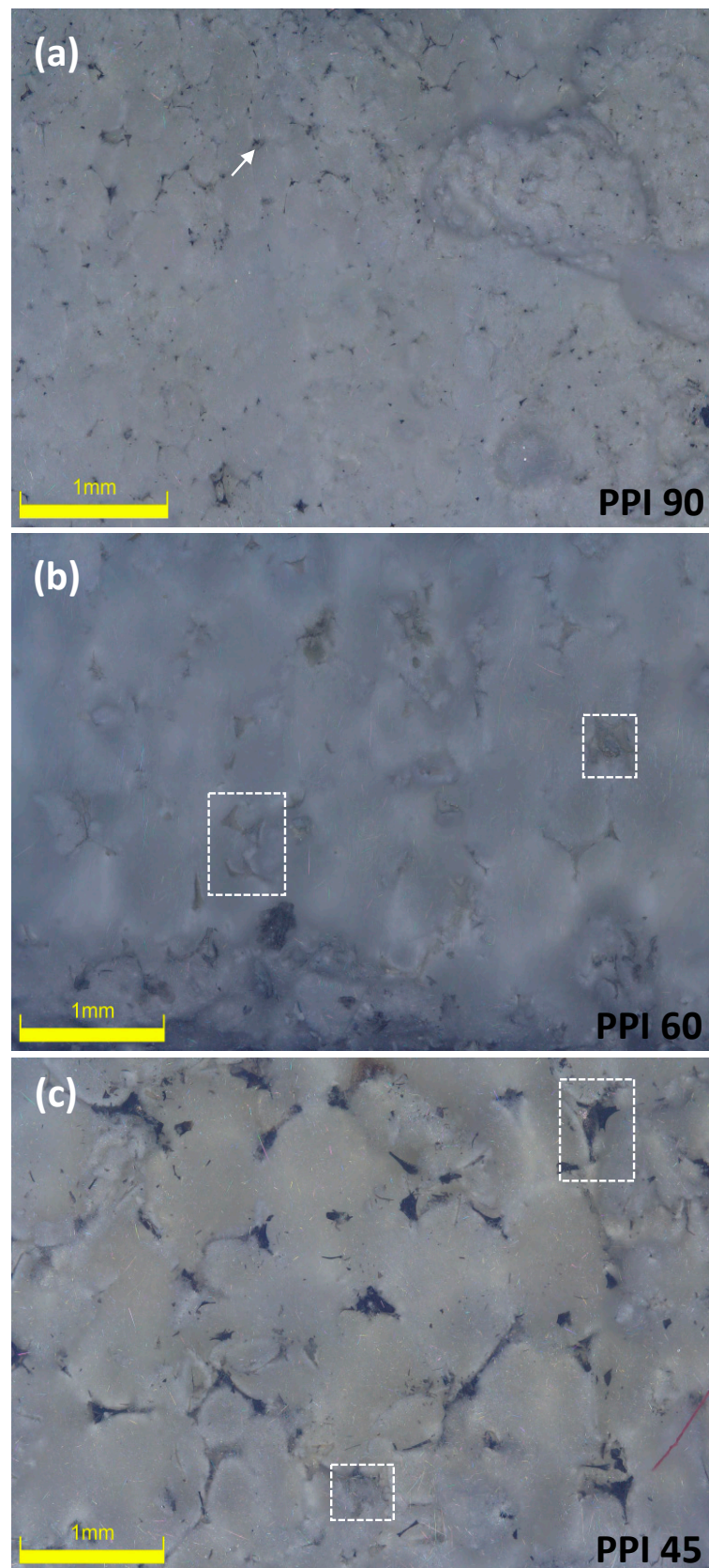**Figure 5.** Digital microscopic images of felts prepared from (**a**) PPI 90, (**b**) PPI 60, and (**c**) PPI 45 at an N_2 flow rate of 600 $cm^3.min^{-1}$ (images from samples prepared using 20 mm PUs; the relicts of the foams are shown in squares and pointed arrow).

The thermal diffusivity (κ) of the felts was measured at three temperatures, viz. RT, 100 °C, and 300 °C. The thermal conductivity (λ) was calculated using the specific heat capacity (Cp) data from [15], κ, and the bulk density (ρ), following the equation $\lambda = \rho * Cp * \kappa$ [18], and the results are presented in Figure 6. In the case of the felts prepared using PPI 45 and PPI 60, the λ computed for the felts prepared at 600 $cm^3.min^{-1}$ (flow rate of N_2) was lower than that of the ones prepared at 100 $cm^3.min^{-1}$. However, in the case of PPI 90, the λ calculated showed only marginal variation. The presence of a low-conducting phase in the felts (the unconverted foam relicts that appear as dark regions (see Figures 3 and 4)), prepared at a higher flow rate, could lower the total λ by forming an extra interface in the conducting matrix. However, more investigation is needed to explain this observation.
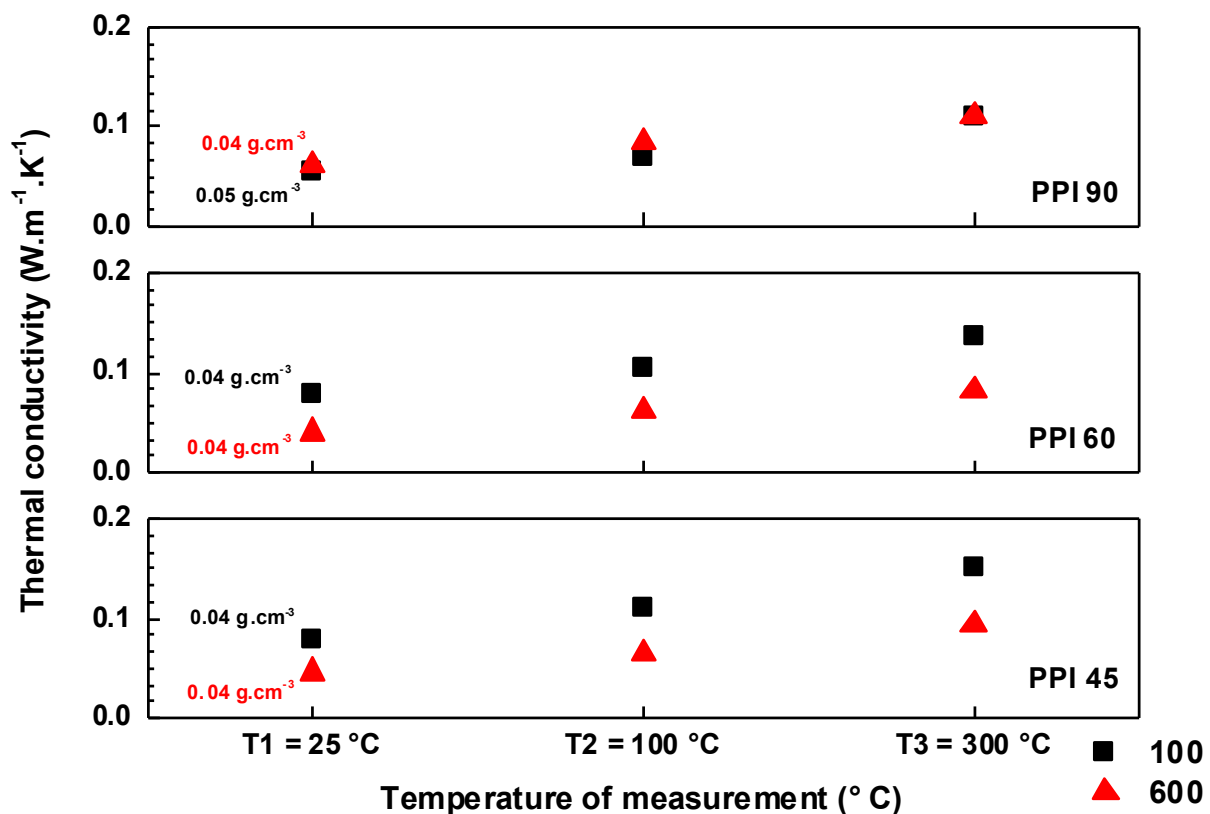

Figure 6. Thermal conductivity of the felts prepared from PPI 45, PPI 60, and PPI 90. The thermal diffusivity was measured in an N_2 environment on the felts prepared from 10 mm PUs, and the measurements were taken at RT (25 °C), 100 °C, and 300 °C.

The dark relicts can be seen in all the felts samples from all three PPIs (45, 60, and 90) at a higher flow rate (600 $cm^3.min^{-1}$) (see Figure 3); however, the influence was more protuberant in the case of the lower PPIs (45 and 60). The microscopic and SEM observation agrees with this remark (see Figures 4 and 5); the transformation in PPI 90 is better despite the different flow conditions (N_2 flow rate) (i.e., a lesser amount of relicts remained in the case of felts from PPI 90 at a 600 $cm^3.min^{-1}$ flow in comparison to PPI 45 and PPI 60 at 600 $cm^3.min^{-1}$).

4. Conclusions

The influences of N_2 gas and the gas flow rates on the evolution and transformation of ultra-light Si_3N_4 nano-belts, synthesized via a PDC approach, by the controlled pyrolysis of polysiloxane-impregnated PU foams, were testified. The samples were made following the previously optimized and reported preparation conditions: 1565 °C/4 h/N_2-atmosphere. The study was conducted using two different flow rates; 100 $cm^3.min^{-1}$ (low-flow) and 600 $cm^3.min^{-1}$ (high-flow) evidenced that the low flow rates (100 $cm^3.min^{-1}$, which

corresponds to a N$_2$ flux of ~2.60 cm.min^{-1} at the cross-section of the furnace) favored a better transformation of the foam → felt. The high flow of N$_2$ gas washed away the reactive gases such as SiO, formed during the process, which were vital for the nanobelt formations. The smaller cell sizes of the PU templates (PPI 90) also favored the nano-felts transformation even at higher gas flow rates compared to the ones with bigger cell sizes used in the study (PPI 45 and 60).

Supplementary Materials: The following supporting information can be downloaded at: https://www.mdpi.com/article/10.3390/ma15031068/s1, Figure S1: Pictures of felt samples prepared from different PU PPIs at a N$_2$ flow rate of 300 cm^3.min^{-1}: (a) top view, and (b) side view (demonstrated using samples prepared using 10 mm PUs with a SPR 036: PU (by wt.) = 2:1); Table S1: The dimensions of the starting PU foams; Table S2: The bulk density, volumetric shrinkage, and mass loss (%) of nano-felts samples prepared with different PPIs at flow rates 100 cm^3.min^{-1}, 300 cm^3.min^{-1}, and 600 cm^3.min^{-1} having varied thickness.

Author Contributions: Conceptualization, B.S. and G.D.S.; Data curation, B.S. and A.Z.; Formal analysis, B.S. and A.Z.; Investigation, B.S., M.B. and A.Z.; Methodology, B.S., M.B. and A.Z.; Resources, G.D.S.; Supervision, G.D.S.; Validation, M.B. and A.Z.; Visualization, B.S.; Writing—original draft, B.S.; Writing—review & editing, M.B., A.Z. and G.D.S. All authors have read and agreed to the published version of the manuscript.

Conflicts of Interest: The authors declare no conflict of interest.

References

1. Kingery, W.D.; Bowen, H.K.; Uhlmann, D.R. *Introduction to Ceramics*; John Wiley & Sons: Hoboken, NJ, USA, 1976; Volume 17, ISBN 0-471-47860-1.
2. Lu, D.; Su, L.; Wang, H.; Niu, M.; Xu, L.; Ma, M.; Gao, H.; Cai, Z.; Fan, X. Scalable Fabrication of Resilient SiC Nanowires Aerogels with Exceptional High-Temperature Stability. *ACS Appl. Mater. Interfaces* **2019**, *11*, 45338–45344. [CrossRef] [PubMed]
3. Si, Y.; Wang, X.; Dou, L.; Yu, J.; Ding, B. Ultralight and Fire-Resistant Ceramic Nanofibrous Aerogels with Temperature-Invariant Superelasticity. *Sci. Adv.* **2018**, *4*, eaas8925. [CrossRef] [PubMed]
4. Wang, H.; Zhang, X.; Wang, N.; Li, Y.; Feng, X.; Huang, Y.; Zhao, C. Ultralight, Scalable, and High-Temperature–Resilient Ceramic Nanofiber Sponges. *Sci. Adv.* **2017**, *3*, e1603170. [CrossRef] [PubMed]
5. Xu, X.; Zhang, Q.; Hao, M.; Hu, Y.; Lin, Z.; Peng, L.; Wang, T.; Ren, X.; Wang, C.; Zhao, Z.; et al. Double-Negative-Index Ceramic Aerogels for Thermal Superinsulation. *Science* **2019**, *363*, 723–727. [CrossRef] [PubMed]
6. Hrubesh, L.W. Aerogel Applications. *J. Non-Cryst. Solids* **1998**, *225*, 335–342. [CrossRef]
7. Santhosh, B.; Vakifahmetoglu, C.; Ionescu, E.; Reitz, A.; Albert, B.; Sorarù, G.D. Processing and Thermal Characterization of Polymer Derived SiCN(O) and SiOC Reticulated Foams. *Ceram. Int.* **2020**, *46*, 5594–5601. [CrossRef]
8. Jana, P.; Zera, E.; Sorarù, G.D. Processing of Preceramic Polymer to Low Density Silicon Carbide Foam. *Mater. Des.* **2017**, *116*, 278–286. [CrossRef]
9. de Guinoa, A.S.; Zambrana-Vasquez, D.; Alcalde, A.; Corradini, M.; Zabalza-Bribián, I. Environmental Assessment of a Nano-Technological Aerogel-Based Panel for Building Insulation. *J. Clean. Prod.* **2017**, *161*, 1404–1415. [CrossRef]
10. Dong, S.; Hu, P.; Zhang, X.; Cheng, Y.; Fang, C.; Xu, J.; Chen, G. Facile Synthesis of Silicon Nitride Nanowires with Flexible Mechanical Properties and with Diameters Controlled by Flow Rate. *Sci. Rep.* **2017**, *7*, 45538. [CrossRef]
11. Lu, J.; Guo, K.; Song, Q.; Li, Y.; Zhang, L.; Li, H. In-Situ Synthesis Silicon Nitride Nanowires in Carbon Fiber Felts and Their Effect on the Mechanical Properties of Carbon/Carbon Composites. *Mater. Des.* **2016**, *99*, 389–395. [CrossRef]
12. Li, D.; Guzi de Moraes, E.; Guo, P.; Zou, J.; Zhang, J.; Colombo, P.; Shen, Z. Rapid Sintering of Silicon Nitride Foams Decorated with One-Dimensional Nanostructures by Intense Thermal Radiation. *Sci. Technol. Adv. Mater.* **2014**, *15*, 045003. [CrossRef] [PubMed]
13. Kaloyeros, A.E.; Jové, F.A.; Goff, J.; Arkles, B. Silicon Nitride and Silicon Nitride-Rich Thin Film Technologies: Trends in Deposition Techniques and Related Applications. *ECS J. Solid State Sci. Technol.* **2017**, *6*, P691. [CrossRef]

14. Su, L.; Li, M.; Wang, H.; Niu, M.; Lu, D.; Cai, Z. Resilient Si$_3$N$_4$ Nanobelt Aerogel as Fire-Resistant and Electromagnetic Wave-Transparent Thermal Insulator. *ACS Appl. Mater. Interfaces* **2019**, *11*, 15795–15803. [CrossRef] [PubMed]

15. Biesuz, M.; Zera, E.; Tomasi, M.; Jana, P.; Ersen, O.; Baaziz, W.; Lindemann, A.; Sorarù, G.D. Polymer-Derived Si3N4 Nanofelts for Flexible, High Temperature, Lightweight and Easy-Manufacturable Super-Thermal Insulators. *Appl. Mater. Today* **2020**, *20*, 100648. [CrossRef]

16. Tong, Z.; Zhang, B.; Yu, H.; Yan, X.; Xu, H.; Li, X.; Ji, H. Si$_3$N$_4$ Nanofibrous Aerogel with In Situ Growth of SiO$_x$ Coating and Nanowires for Oil/Water Separation and Thermal Insulation. *ACS Appl. Mater. Interfaces* **2021**, *13*, 22765–22773. [CrossRef] [PubMed]

17. Gao, F.; Yang, W.; Fan, Y.; An, L. Mass Production of Very Thin Single-Crystal Silicon Nitride Nanobelts. *J. Solid State Chem.* **2008**, *181*, 211–215. [CrossRef]

18. Santhosh, B.; Ionescu, E.; Andreolli, F.; Biesuz, M.; Reitz, A.; Albert, B.; Sorarú, G.D. Effect of Pyrolysis Temperature on the Microstructure and Thermal Conductivity of Polymer-Derived Monolithic and Porous SiC Ceramics. *J. Eur. Ceram. Soc.* **2021**, *41*, 1151–1162. [CrossRef]

19. Semerci, T.; de Mello Innocentini, M.D.; Marsola, G.A.; Lasso, P.R.O.; Soraru, G.D.; Vakifahmetoglu, C. Hot Air Permeable Preceramic Polymer Derived Reticulated Ceramic Foams. *ACS Appl. Polym. Mater.* **2020**, *2*, 4118–4126. [CrossRef]

20. Valentini, F.; Dorigato, A.; Pegoretti, A.; Tomasi, M.; Sorarù, G.D.; Biesuz, M. Si$_3$N$_4$ Nanofelts/Paraffin Composites as Novel Thermal Energy Storage Architecture. *J. Mater. Sci.* **2021**, *56*, 1537–1550. [CrossRef]

21. Biesuz, M.; Tomasi, M.; Santhosh, B.; Sglavo, V.M.; Sorarù, G.D. Polymer-Derived Si3N4 Nanofelts as a Novel Oil Spills Clean-up Architecture. *J. Environ. Chem. Eng.* **2020**, *8*, 104134. [CrossRef]

22. Sorarù, G.D.; Girardini, K.; Narisawa, M.; Biesuz, M. Effect of Anionic Substitution on the High Temperature Stability of Polymer-derived SiOC Glasses. *J. Am. Ceram. Soc.* **2021**, *104*, 3097–3104. [CrossRef]

23. Wei, Q.; Pippel, E.; Woltersdorf, J.; Scheffler, M.; Greil, P. Interfacial SiC Formation in Polysiloxane-Derived Si–O–C Ceramics. *Mater. Chem. Phys.* **2002**, *73*, 281–289. [CrossRef]